Optical Phase Modulators for MHz and GHz Modulation in Silicon-On-Insulator (SOI)

Ching Eng Png, Seong Phun Chan, Soon Thor Lim, and Graham T. Reed

***Abstract*—This paper reports the simulation of the direct current (dc), transient, and optical characteristics of low-loss single-mode optical phase modulators based on silicon-on-insulator (SOI) material. The devices operate by injecting free carriers to change the refractive index in the guiding region and have been modeled using the two-dimensional (2-D) device simulation package SILVACO and the optical simulator BeamPROP to determine their electrical and optical performance, respectively. These simulators have been employed to optimize the overlap between the injected free carriers in the intrinsic region and the propagating optical mode. Attention has been paid to both the steady state and transient properties of the device. In order to produce quantitative results, a particular *p-i-n* device geometry has been employed in the study, but the trends in the results are sufficiently general to be of help in the design of many modulator geometries. The specific example devices used are designed to support a single optical guided mode and are of approximately 1 μm in cross-sectional dimensions. The modeling results predict that the transient performance of the device is affected significantly by the contact width and the rib doping depth. Results presented encompass Gaussian and constant doping profiles in the n^+ regions. The doping profile of the contacts has a tremendous effect on both the dc and transient performances. Phase modulators with drive currents as low as 0.5 mA and transient rise times of 0.3 ns and fall times of 0.12 ns are predicted. Following from these results, a realistic doping profile is proposed that surpasses the electrical results of the Gaussian and most of the constant doping profiles. The improvements in electrical device characteristics are at the expense of a slightly increased optical absorption loss. An alternative switching technique is also presented that could further improve the device speed.**

***Index Terms*—Carrier injection, optical phase modulator, plasma dispersion effect, rib waveguides, silicon-on-insulator (SOI), silicon photonics.**

I. Introduction

OPTICAL switches and modulators are essential components for some integrated optics applications. In this paper, we report the design of variants of a high-speed, small-geometry (0.98 μm) optical phase modulator based on the plasma dispersion effect, through analyzing a particular geometry of the modulator using the two-dimensional (2-D) semiconductor simulation package SILVACO [1]. Various aspects of this geometry, such as side contact width and side dopant displacement from the rib edges, are also varied to enable a better understanding of the device. While the results are specific to the chosen device geometry, some of the results are sufficiently general to enable improvement in the performance of many other device geometries. A number of design parameters of the modulators are discussed, including the optimum configuration of a three terminal p-i-n diode around a rib waveguide, and the optimization of both the power efficiency and the operating speed of the device, for various doping profiles in the n^+ regions.

In recent years, there has been a significant interest in the development of optical waveguide modulators and switches using silicon-on-insulator (SOI) substrates, motivated by the potential to provide a reliable low-cost alternative to other materials for fiber-based local access systems as well as a number of other applications (e.g., [2]–[4]). The main reasons why SOI has proven successful for integrated optics are that the material and the processing are relatively low cost with resulting waveguides having a loss as low as 0.15 dB/cm (e.g., [5] and [6]). The SOI structure is strongly confining. A rib structure leads to vertical confinement of the optical mode as a result of the high-refractive-index difference between the air/silicon/SiO_2 and horizontal confinement results from the etched rib, enabling bends and interconnections to be produced much more easily than in structures that confine the optical mode less well.

Until recently, the majority of researchers concentrated on devices with silicon surface-layer thicknesses of the order of several microns, hence resulting in low-loss waveguides and easy coupling to and from the outside world. However, optical phase modulators based on overlayer thicknesses of several microns are limited to modest modulation bandwidths of the order of 10–20 MHz (e.g., [7] and [8]).

In order to increase the speed of these devices, it is desirable to reduce the dimensions of the waveguides upon which the modulators are based and, hence, the silicon overlayer thickness of the SOI wafer [9].

II. Modulation Mechanism

Soref and Bennet produced the following extremely useful expressions relating the refractive index and absorption coefficients changes in silicon [10] due to injection or depletion of carriers in silicon [11], which are now widely used:

$$\begin{aligned}&\text{At } \lambda = 1.55\ \mu\text{m}:\\ &\Delta n = \Delta n_e + \Delta n_h\\ &\quad = -8.8\times10^{-22}(\Delta N_e) - 8.5\times10^{-18}(\Delta N_h)^{0.8} \quad (1)\end{aligned}$$

Manuscript received July 22, 2003; revised February 2, 2004. The work of C. E. Png was supported in part by the Overseas Research Student (ORS) Award Scheme, Bookham Technology, Inc., and the Institution of Electrical Engineers (IEE). The work of S. P. Chan and S. T. Lim was supported in part by Agilent Technologies (Singapore) and the University of Surrey, Surrey, U.K.

The authors are with the Advanced Technology Institute, School of Electronics and Physical Sciences, University of Surrey, Guildford, Surrey GU2 7XH, U.K. (e-mail: j.png@surrey.ac.uk).

Digital Object Identifier 10.1109/JLT.2004.827655

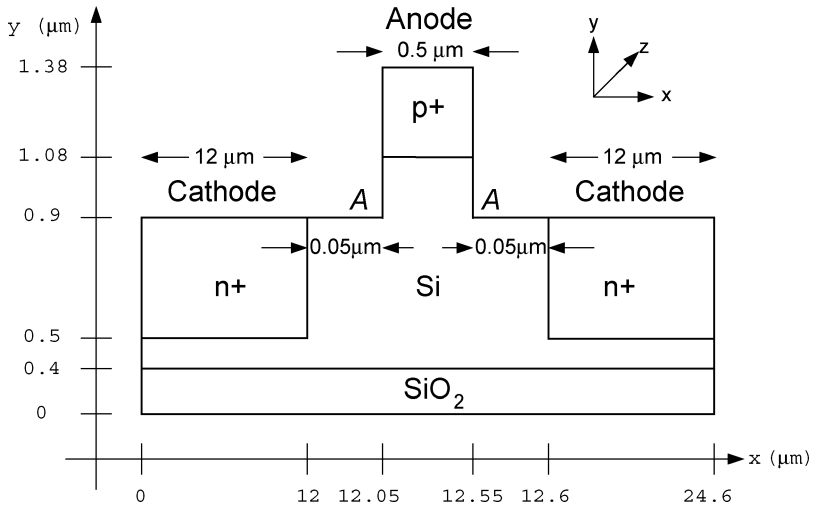

Fig. 1. Geometry of the reference model (RM) p-i-n phase modulator.

$$\Delta\alpha = \Delta\alpha_e + \Delta\alpha_h = 8.5\times10^{-18}(\Delta N_e) + 6.0\times10^{-18}(\Delta N_h) \quad (2)$$

where

- λ the free-space wavelength;
- Δn_e the change in refractive index resulting from change in free electron-carrier concentrations;
- Δn_h the change in refractive index resulting from change in free hole-carrier concentrations;
- $\Delta\alpha_e$ the change in absorption resulting from change in free electron-carrier concentrations;
- $\Delta\alpha_h$ the change in absorption resulting from change in free hole-carrier concentrations.

From (1), it is noted that the refractive index decreases as the concentration of injected carriers increases. Furthermore, from (1) and (2), notice that a finite change in the silicon refractive index must also result in a finite change in the absorption of the silicon, and further, the absorption loss due to electrons is greater than that for holes. A change in the carrier density can be achieved by forward biasing a silicon p-i-n diode fabricated around the rib waveguide (Fig. 1).

III. Device Structure

Fig. 1 shows the generic device structure to be considered in this paper. It is a lateral optical phase modulator integrated into a low-loss SOI rib waveguide. The device shown in Fig. 1 will be referred to as the reference model (RM), such that any variations in the geometry of the device or doping profiles/concentrations are implicitly to be compared with the reference modulator in order to demonstrate an improvement or a degradation in a device performance. The RM in Fig. 1 represents the geometry used in all simulations unless otherwise stated.

The device has a symmetrical p-i-n structure where two n^+ regions are joined as a common cathode. In the reference device, both n and p regions were modeled as highly doped regions with constant doping concentrations of 10^{20} cm^{-3}. These devices were based around an overall silicon thickness of 0.98 μm, etched rib waveguides 0.5 μm wide with an etch depth of 0.48 μm in order to satisfy the single-mode condition [12]. The oxide thickness was modeled to be 0.4 μm to ensure sufficiently good optical confinement.

IV. Electrical and Optical Analysis

The ATLAS device simulation package from SILVACO [1] has been used to predict the electrical characteristics of the modulator. These include dc and transient characteristics. This 2-D simulator is physically based and predicts the device electrical characteristics by solving semiconductor physics equations related to the device physical structure, such as Poisson's equation, and the charge continuity equations for holes and electrons. The simulator has been used to predict the injected free-carrier concentrations in the intrinsic region of the devices for both dc and transient biasing conditions. The change in concentration of free carriers is then converted to refractive index change in the device by using (1) determined by Soref and Bennett [10]. Such a simulator allows predictions of internal physical mechanisms, which are difficult to determine experimentally. This simulator is utilized here to enable a prediction of the injected free-carrier density under a range of different working conditions and device geometries.

This approach has been validated in the past by experimental verification of predicted device performance (e.g., [8] and [13]). A change in refractive index of the silicon guiding layer results from an injection of free carriers into the guiding region. In order to maximize this change, we must optimize the interaction between the injected free carriers and the propagating optical mode.

The simulator does not provide a prediction of the overlap integral between the electrical carriers and the optical field. However, it will be shown that there exists a high degree of uniformity in the predicted injected carrier concentration at the levels of interests throughout the central guiding region of the device. This will clearly result in a uniform refractive index change across the waveguiding region. Therefore, we can obtain from SILVACO the mean value of the injected carrier concentration in the guiding region and apply the results to (1) and (2) to obtain the resulting changes in refractive index and absorption for the device under investigation, at a wavelength of $\lambda = 1.55$ μm.

Alternatively, the data from the electrical simulation could be transferred to a similar grid-based optical simulator to predict absorption and refractive-index changes, but due to the uniform nature of the injected charge, there should be a negligible difference between these approaches. The change in refractive index results in a phase shift $\Delta\phi$ in the optical mode given approximately by

$$\Delta\phi \approx \frac{2\pi\Delta nL}{\lambda} \tag{3}$$

where L is the active length of the modulator in the z-direction and Δn is the change in refractive index due to injected carriers. Thus, we can estimate the length required to produce a π-phase shift as

$$L_\pi = \frac{\lambda}{2\Delta n}. \tag{4}$$

Alternatively, we can rearrange (4) for Δn and determine the required refractive-index change and, hence, the required carrier density to achieve a π-phase shift for a fixed device length.

V. Simulation Results

The optical wavelength λ and the interaction length in the z direction in all the simulations were assumed to be 1.55 and 500 μm, respectively.

A. Reference Modulator

1) Modeling Characteristics: The device was modeled assuming ohmic contacts with no additional contact resistance or capacitance. The Shockley–Reed–Hall recombination carrier lifetime in the intrinsic region are $\tau_n = 700$ ns, $\tau_p = 300$ ns, where τ_n and τ_p are the electron and hole lifetimes, respectively. The values of τ_n and τ_p correspond to a realistic intrinsic epilayer doping concentration of 10^{15} cm^{-3}; under forward bias, SILVACO adjusts the lifetime according to carrier concentrations [15]. It is expected that a device with shorter intrinsic carrier lifetimes than that stated previously will have superior switching capabilities, but this is at the expense of greater electrical current. Conversely, a device with longer intrinsic carrier lifetimes will have lower power consumption but slower switching capabilities. One method of reducing the carrier lifetime of the intrinsic region is to include a lifetime killer, such as gold, but at the risk of CMOS incompatibility.

2) Phase Modulation and Absorption: Fig. 2 shows the dc change in refractive index plotted against drive current for the reference device in Fig. 1, with a π radian drive current, $I_\pi = 1.48$ mA and a corresponding current density of 592 A/cm^2. I_π is a typical measure of the quality of such devices. This predicted current is an improvement in the experimental dc performance of over 370% over that of Tang *et al.*, where their devices operated in the order of $I_\pi = 7$ mA [8].

From Fig. 2, we can see that the change in refractive index varies nonlinearly with applied current. One factor that contributes to the nonlinearity of the change in refractive index versus current density relation is the sublinear dependence of the change in free holes, ΔN_h with the change in refractive index, as shown in (1). In addition, as we drive the modulator harder, we inject more free carriers into the intrinsic region of the device. This increase in the concentration of the previously intrinsic region results in an increase in the Auger recombination rate (at injected carrier concentrations much greater than 10^{17} cm^{-3}, the Auger recombination becomes the dominant recombination process, e.g., [13]). This results in a reduced lifetime in this region and, hence, we have to drive the modulator harder to achieve an equivalent refractive-index change than at lower drive powers. Of course, an increase in the recombination rate will result in a faster switching device, i.e., reduction in the rise and fall times of the modulator.

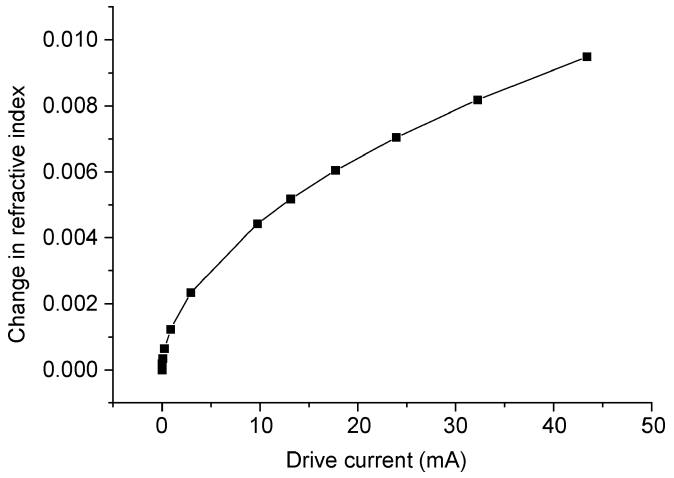

Fig. 2. Change in refractive index against drive current in the RM.

3) Switching Characteristics: The switching characteristics of the reference model in Fig. 1 were evaluated using a transient modeling solution. For the transient solutions, both anode and cathode were first zero biased for 10 ns, followed by a step increase to V_π for 200 ns and a subsequent step decrease to 0 V. V_π is the voltage corresponding to 180° phase shift. The rise time t_r is defined as the time required for the induced phase shift to change from 10% to 90% of the maximum value. Likewise, the fall time t_f is defined as the time required for the induced phase shift to change from 90% to 10% of the maximum value. Unless otherwise stated, all subsequent transient solutions will be subjected to this square waveform. For the reference model, the rise and fall times were determined to be $t_r = 0.51$ ns and $t_f = 0.14$ ns, respectively. Fig. 3 shows the rise and fall times, and it is clear that the rise time is the slower of the two and, hence, the limiting transition. In order to illustrate clearly both the rise and fall times, a "break" in the horizontal time axis was made so that the rising and falling edge of the transient waveform could be highlighted.

4) Injected Free Carriers in the Intrinsic Region: Fig. 4 shows predictions of the injected electron and hole concentrations along a vertical section through the centre of the rib of the reference model. The applied voltage is at 1.00, 0.92, and 0.84 V for the upper, middle, and lower plots, respectively. The injected plasma shows good uniformity in the intrinsic region for the applied forward biases of interest. The maximum variation in the concentration of the injected carriers through the center of the waveguiding region is seen to be less than 1%. Fig. 5 illustrates a similar cutline applied in the horizontal

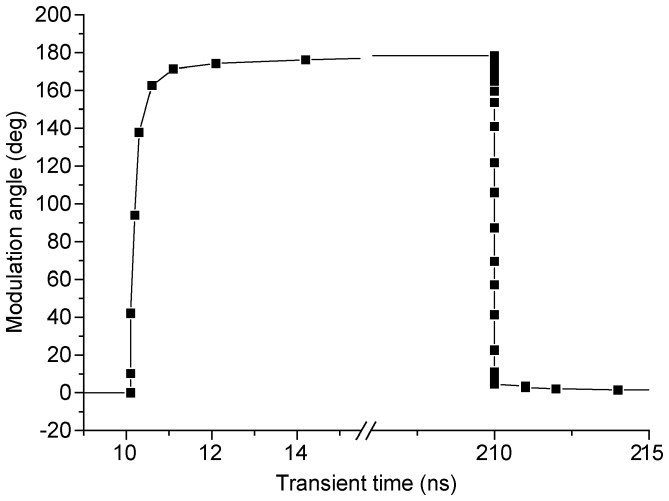

Fig. 3. Predicted transient performance for the reference modulator.

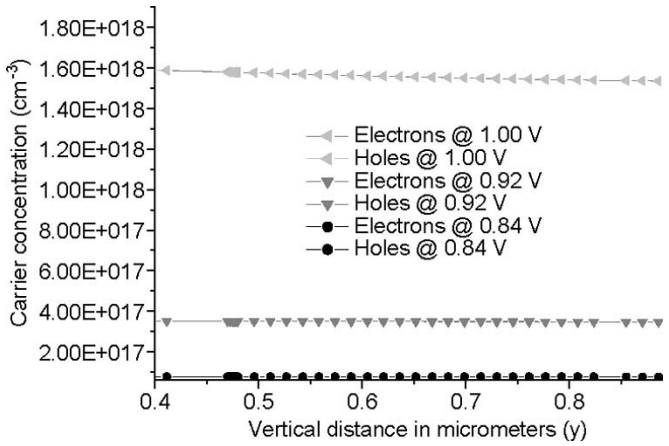

Fig. 4. Injected free carriers along a vertical section ($x = 12.3\ \mu$m) for the reference model.

direction, which also predicts good carrier density uniformity. Therefore, it is justifiable to make the assumption of a constant profile of injected carriers in the intrinsic region for the range of voltage biases of interest. From Fig. 4, we can see that it should be relatively easy to produce injection density levels (electrons and holes) of 5×10^{17} cm^{-3} and, in turn, we can calculate the length L needed to achieve a π phase.

Using (4), we can approximate the length of the designed reference modulator needed to produce a π-phase shift at this level of injection to be 465 μm. Obviously, if the injection level is higher, L can be reduced.

B. Device Characteristics for the Modulator With Rounded Edges

This section considers the effect of rounded edges at the base of the rib, which may occur during fabrication of a real device. The curvature occurs at points A in Fig. 1 with radius of curvature R. Values of R used are 25 and 50 nm, as depicted in Fig. 6. The results indicate a slight improvement in device performance, which appears to be greatest for a radius of curvature $R = 25$ nm. For example, the RM requires a current of 1.48 mA

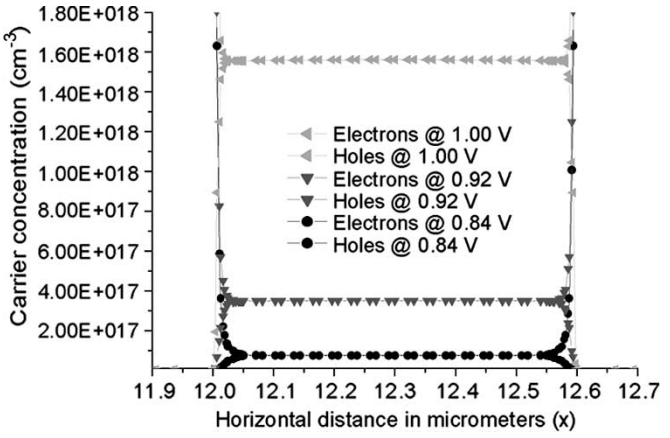

Fig. 5. Injected free carriers along a horizontal section ($y = 0.6\ \mu$m) for the reference model.

to achieve a π-phase shift, whereas for the rounded wall modulator with $R = 25$ nm, a forward current of 1.44 mA is required to achieve a π-phase shift, a slight improvement of 2.7%. Intuitively less crowding of carriers would be expected at a curved corner than at an abrupt corner. This suggests that perhaps more carriers will occupy areas of the waveguide in which the optical mode propagates, although this is likely to be a small effect. The drive current required when $R = 50$ nm is similar to the device with $R = 25$ nm.

There is an improvement of 17% in the rise time for the rounded wall modulator with $R = 25$ nm when compared with the reference modulator (0.43 versus 0.51 ns), whereas the fall time does not exhibit significant change (0.15 versus 0.14 ns). The rise and fall times when $R = 50$ nm are 0.45 and 0.16 ns. Overall, the results indicate that both the dc and transient performance of the modulator can be influenced slightly by the small change from a straight rib wall to one that has a small radius of curvature at the rib base.

C. Doping Distribution

As the optical phase modulators reported here utilize the free-carrier plasma dispersion effect, the doping distributions have a tremendous influence on device performance parameters, such as drive current and operating speed. Aspects investigated include the doping concentrations, doping depths, and doping profiles of the p^+ and n^+ regions.

1) Effect of Side (n) Dopant Depth: The depth of the contact doping has a significant impact on the modulator performance. In Fig. 1, the RM has a side contact depth of 0.4 μm heavily doped with donors at 10^{20} cm^{-3}. The RM requires a forward drive current of 1.48 mA to achieve a π-phase shift (I_π), whereas the modulator with the shallower doping depth of 0.2 μm requires $I_\pi = 2.4$ mA. Hence, there is an increase in the current consumption of 60% when the side contact depth is shallower. Conversely, I_π is reduced by 200% when the contact depth is even deeper than in the RM (0.5 μm). Fig. 7 displays these results graphically.

The transient response also yields improvements in the rise and fall times of the modulators with deeper doping. The rise and fall times were 1.5 and 0.34 ns, respectively, for the modulator with the shallower doping depth (0.2 μm), whereas the

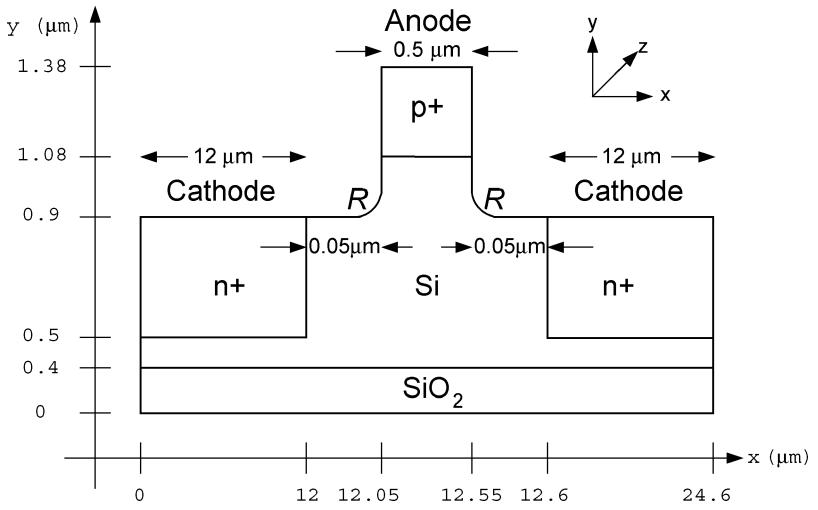

Fig. 6. Geometry of the reference modulator with curvature points at the base of the rib edges. The curvature radii R were simulated to be 25 and 50 nm.

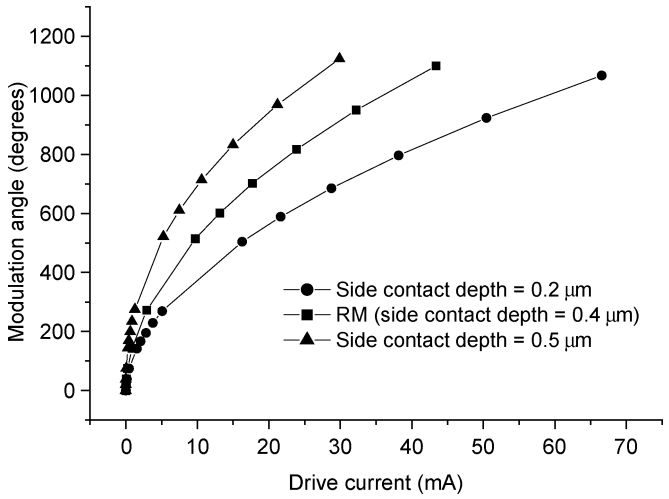

Fig. 7. Phase modulation versus drive current for various side-doping contact depths.

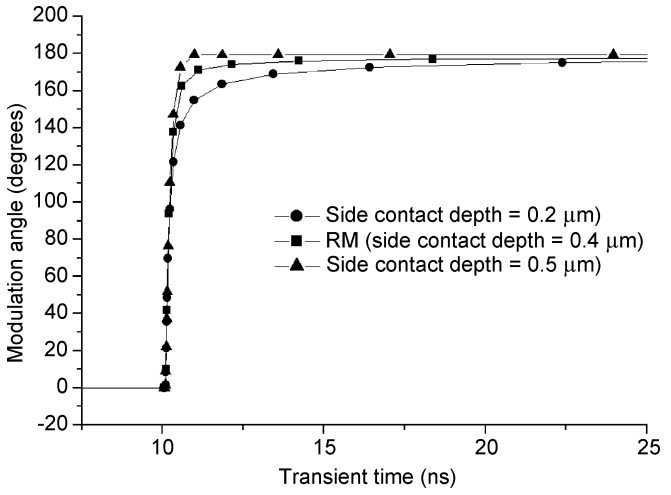

Fig. 8. Phase modulation versus transient time for various side-doping contact depths.

rise and fall times for the modulator with the deeper dopants (0.5 μm) decreased to 0.3 and 0.12 ns, respectively. Fig. 8 shows the rise times.

The increase in both the dc and transient performance with increasing doping depth is partly due to the increase in the number of free electrons and holes, which are available for injection in to the guiding region, because increasing the dopant depth increases the area of the injection contact adjacent to the waveguiding region. A shallow doping depth also tends to result in a larger proportion of the injected carriers residing in the area directly below the doping regions, where little of the optical mode exists.

These calculations were made for constant concentration profiles. In a real device, the concentration profiles will vary, but the trends regarding the depth of doping will still be applicable, suggesting that the deepest doping possible is desirable. However, the disadvantage in a deep doping region is an increase in the complexity and time of the fabrication process.

2) Effect of Top-Rib Doping Depth: Varying the top-rib doping depth while keeping the remainder of the parameters unchanged showed that the rib doping depth has a very significant impact on the modulation speed [14]. For example, when the doping depth is decreased from 0.3 to 0.1 μm, the rise time increased from 0.51 to 0.99 ns, respectively. This, in turn, implies that the modulation speed decreased from 980 to 500 MHz. The fall time also increased from 0.14 to 0.36 ns, with a reduction in top-rib dopant depth. The drive current I_π remains at approximately 1.5 mA for both doping depths. However, the optical attenuation increases if the doping depth extends too deeply into the rib.

3) The Effect of Doping Concentration: The concentration of the doping regions also affects the dc and transient performance of the modulator. The doping concentrations of the reference model were constant and, hence, there may be some degradation in real devices due to the difficulty in fabricating such a doping profile.

For a range of different combinations of concentrations ranging from 10^{19} to 10^{20} cm^{-3} in the n^+ contact windows, it is observed that there is an increase in the modulator's dc performance for higher doping concentration. For example, the reference model has doping concentrations of 10^{20} cm^{-3} in both the n^+ and p^+ contact windows. To achieve a π-phase

TABLE I
DEVICE CHARACTERISTICS WHEN THE DOPING CONCENTRATION IS VARIED

Device Model n-p-n (cm^{-3})	Rise time, t_r(ns)	Fall time, t_f(ns)	Drive current, I_π (mA)
10^{19}-10^{20}-10^{19}	0.44	0.15	9.3
10^{19}-10^{19}-10^{19}	0.48	0.15	10.5
10^{20}-10^{20}-10^{20} (RM)	0.51	0.14	1.5
10^{20}-10^{19}-10^{20}	0.54	0.16	2.5

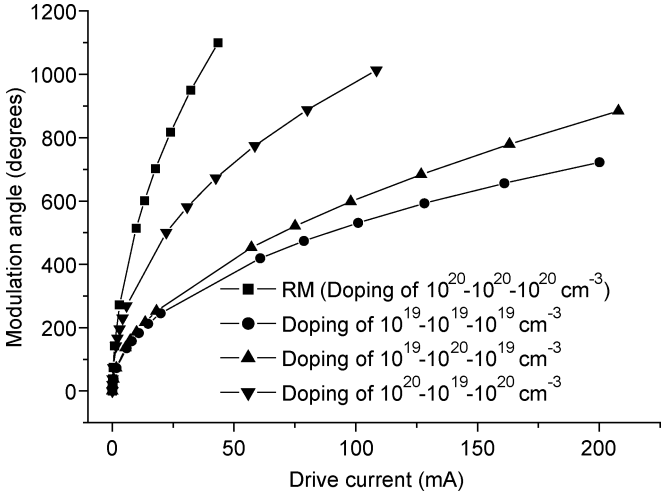

Fig. 9. Phase modulation versus drive current for various doping concentration levels.

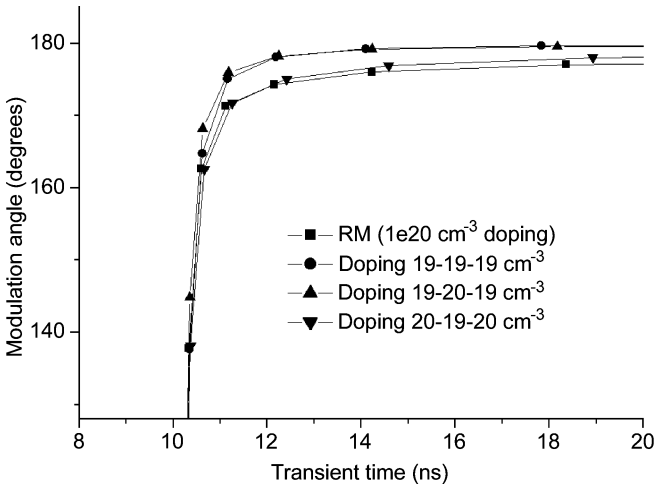

Fig. 10. Phase modulation versus transient time for various doping concentration levels.

shift for a modulator of 500-μm interaction length, a forward current of 1.48 mA is required. For a similar device with doping concentrations that are an order of magnitude lower (i.e., 10^{19} cm^{-3}), a forward current of 10.5 mA is required to achieve a π-phase shift for a modulator of 500-μm interaction length. Consequently, there is an increase in the current required for a π-phase shift by a factor of seven for the modulator with lower doping concentration. Fig. 9 shows these dc results graphically.

Interestingly, reducing the doping concentration results in a slight decrease in the rise time of the modulator, while the fall time remains almost unchanged. For the two devices compared previously, t_r was 0.51 ns for the reference model, which has a higher doping concentration, and 0.44 ns for the lower doping concentration device, while the fall times t_f are 0.14 and 0.15 ns, respectively. Fig. 10 shows the transient results, and all the doping concentration results are summarized in Table I.

An increase in the doping concentration of the n^+ and p^+ regions will increase the static absorption of the optical mode that impinges on the n^+ and p^+ regions. In addition, the increase in the doping concentration of the n^+ and p^+ regions will result in a small increase in the refractive-index difference between the intrinsic region and the n^+ and p^+, resulting in slightly stronger confinement of the propagating optical mode in the intrinsic region; therefore, a smaller portion of the optical mode will propagate in the highly doped n^+ and p^+ regions. The static absorption loss is defined as the zero-bias optical propagation loss of the device due to free-carrier absorption of parts of the optical mode profiles that extend into the doped contacts, together with absorption loss due to the low density of carriers in the waveguide core.

The dynamic optical absorption is defined as the optical propagation loss of the device when biased such that a π radian phase shift is induced and is due to the additional absorption loss due to injected electrons and holes. Assuming the number of injected carriers in the waveguiding region is 5×10^{17} cm^{-3}, from (4) the absorption coefficient for the reference model is $\alpha = 7.25$ cm^{-1} (i.e., $\sim$31.5 dB/cm). This would result in a dynamic optical absorption of approximately 1.6 dB if the active device length is 500 μm.

D. Effects Due to the Displacement of the Side-Doping Contacts From the Rib Edges

An evaluation of the modulator performance was made in terms of the displacement of the doping contact windows from the base of the rib. This is represented by the variable "A" in Fig. 1, which was investigated in terms of the device performance.

1) DC Characteristics: The dc results are shown in Fig. 11 and predict that there is an increased performance in terms of induced phase modulation against current if the doping windows are placed close to the center of the waveguide. This is a consequence of the reduction in the distance between the n^+ and p^+ regions. However, with decreasing separation of the n^+ and p^+ regions, the doping in the region where the majority of the optical mode propagates is increased, which will result in an increase in the absorption of the device. If the n^+ and p^+ regions are heavily doped, the optical mode confinement will be slightly

TABLE II
DEVICE CHARACTERISTICS WHEN THE PARAMETER "A" (FIG. 1) IS VARIED

Displacement of parameter 'A' (nm)	Rise time, t_r(ns)	Fall time, t_f(ns)	Drive current, I_π (mA)
50 (RM)	0.51	0.14	1.480
200	0.73	0.19	1.505
300	0.88	0.20	1.511
750	1.90	0.35	1.542

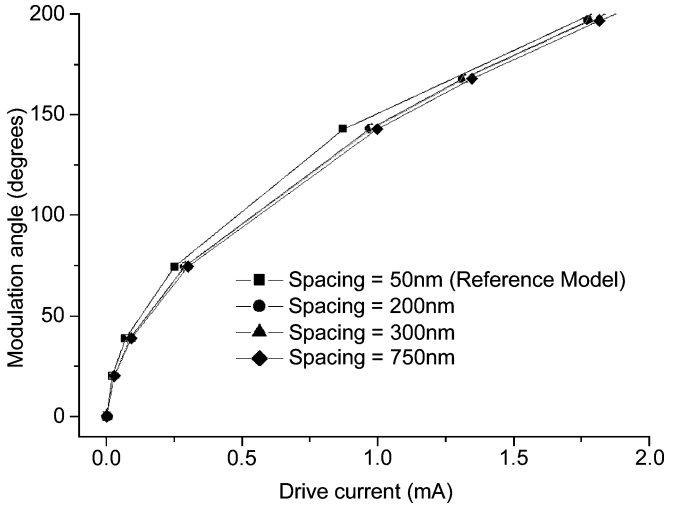

Fig. 11. Phase modulation versus drive current for various contact widths from the sides.

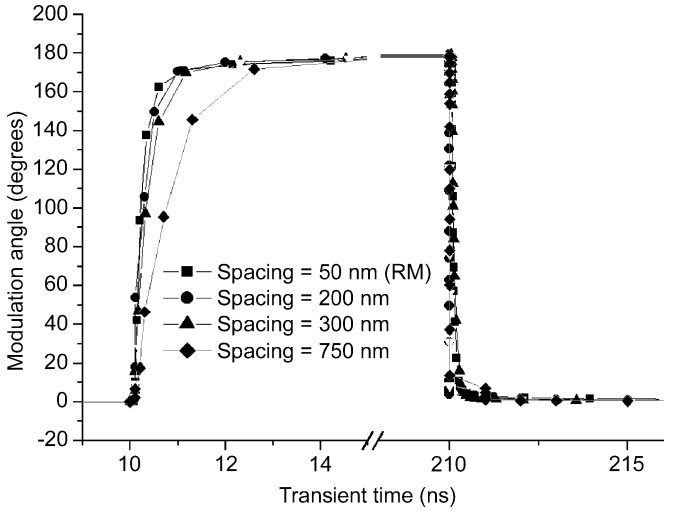

Fig. 12. Phase modulation versus transient time for various dimensions of the variable "A"—the distance between the side contact doping and the rib edge.

enhanced laterally and, hence, absorption due to the tail of the optical mode extending into the n^+ regions will be slightly reduced, although, conversely, the tail of the mode extending into the doped region will suffer increased absorption. The drive current required to produce a π-phase shift for the modulator is predicted to increase by approximately 4% when "A" is varied from 50 (RM) to 750 nm. For applications where low optical attenuation takes precedence over device operating speed, "A" can be increased as the drive current would not increase significantly while reducing optical absorption. However, the device operating speed would reduce with the increase in "A" as discussed in the next section.

2) Switching Characteristics: Fig. 12 shows the phase modulation against time for the modulator with varying values of "A". The applied square-wave input is similar to that described previously. The results indicate that the spacing distance between the doped regions and the rib edge affects the switching characteristics of the modulator more than any other parameter studied in this paper. For example, the device operating speed decreases by over 70% when "A" is increased from 50 to 750 nm. Fig. 12 has a "break" in the horizontal axis in order to display more clearly the rise and fall times. The switching times are summarized in Table II.

Clearly, there is an associated improvement in the lateral confinement of the optical mode when the n^+ regions are translated toward the center of the rib (smaller "A"). Hence, this results in reduced switching times due to the reduction in the time taken to fill or deplete the area where the optical mode now propagates.

The constant doping profile of the contacts shown in Fig. 1 is difficult to fabricate. A more realistic profile would be some sort of graded profile such as a Gaussian doping profile. However, the electrical performance for a device with Gaussian profiles at the side yields inferior characteristics compared with that of the RM, which has a constant side-doping profile. For example, when the side dopant profile is changed from constant to a Gaussian type, I_π increases from 1.48 to 3.72 mA. Likewise, the rise time increases from 0.51 to 1.08 ns, while the fall time stays unchanged at 0.14 ns. In response to this, an achievable side dopant profile that surpasses the performance of the device with the Gaussian doping profile and most of the variants of devices with constant doping profile was also developed. We have called this the *optimum profile*, a term that requires some explanation, because the term *optimum profile* could be interpreted to mean that this profile should provide the best performance. However, it has been shown that a particular constant profile [Section V-C-1] can outperform the optimum profile in terms of both device current and speed. However, the optimum profile provides the best compromise between device performance and a realistic profile that is manufacturable without prohibitively difficult or unrealistic fabrication requirements. This optimum doping profile in the side n^+ regions is achieved through a series of different implantation steps such that the peak concentration at the surface of the n^+ contact is approximately 10^{20} cm^{-3} and decreases to approximately 10^{16} cm^{-3} at the interface between the silicon and the buried oxide. The determination of this profile was achieved through the process simulation package ATHENA from SILVACO [1]. The optimum profile predicts an I_π of 0.7 mA, rise and fall times of 0.38 and 0.13 ns. The dc and transient results for all three different profiles are illustrated in Figs. 13 and 14, respectively.

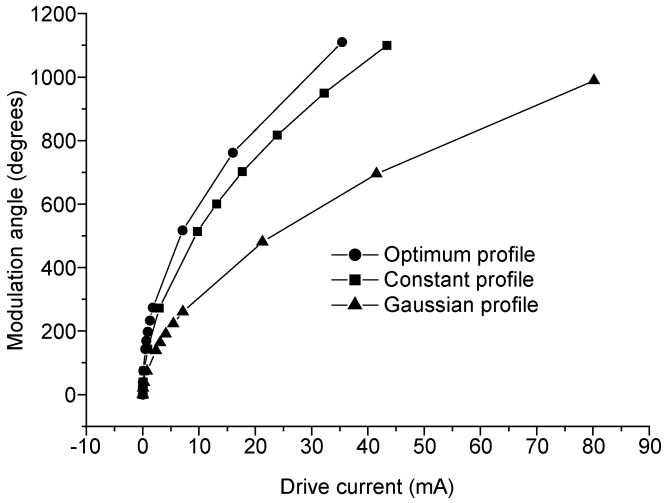

Fig. 13. Phase modulation against drive current in the RM with various doping profiles.

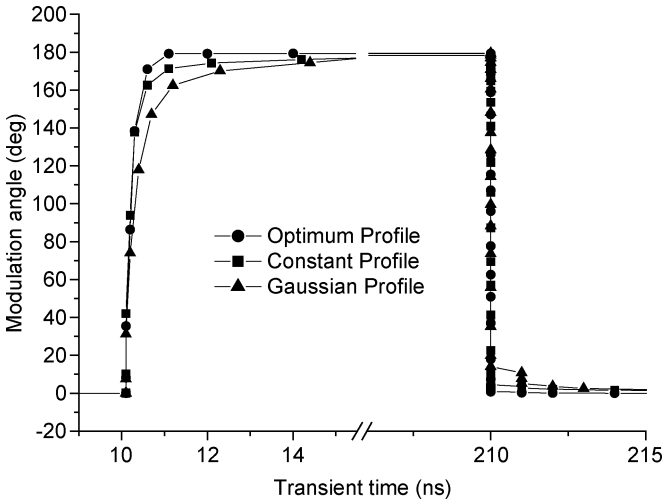

Fig. 14. Predicted transient performance for the RM with various doping profiles.

In this type of silicon-based modulator, phase modulation is always accompanied by some unwanted absorption in the active mode, as described by (2). For example, the unwanted attenuation for a 500-μm-long device with optimized side-doping profile is approximately 1.45 dB ($\sim$28.97 dB/cm) when sufficient carriers are injected to achieve a π radian phase shift.

E. Optical Simulation of the RM

In this section, the effect of polarization and the effects of the side dopant spacing on optical power loss is predicted using BeamPROP, commercially available optical simulation software [16]. The simulations were calculated based on the semi-vectorial beam propagation method (BPM) operating at a wavelength of 1.55 μm. The modeling of the SOI rib waveguide is based on the RM of Fig. 1 with a SiO_2 buried oxide (BOX) layer thickness of 400 nm. The refractive index of the silicon guiding layer is $n_g = 3.477$, and the BOX layer and cladding are $n_s = 1.444$ and $n_c = 1$, respectively. The

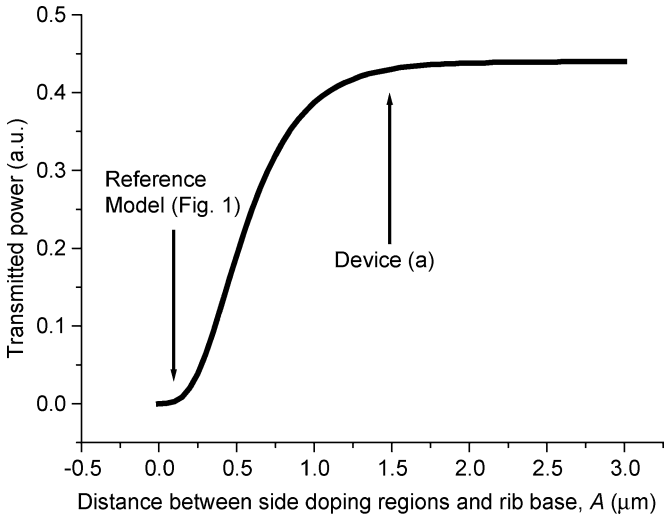

Fig. 15. Optical output power with varying distance between the side-doping regions and the base of the rib.

three-dimensional (3-D) mesh grid spacing used for the BPM simulation are $x = 0.005$ μm, $y = 0.01$ μm, and $z = 0.04$ μm. The inherent high-refractive-index contrast in SOI material enables the realization of submicrometer waveguide without sacrificing the mode confinement and single-mode operation.

When the rib waveguide dimensions are reduced to submicrometer levels, high scattering loss is dominated by the waveguide sidewall roughness and must be addressed. The relationship between waveguide losses, and waveguide dimensions had been studied extensively to enable the design and fabrication of waveguide in SOI with minimal loss (e.g., [17] and [18]), where 0.1-dB/cm transmission loss was demonstrated for a device that is 200 nm in Si height [18]. This reaffirms that the RM, which is 980 nm in Si height, is feasible.

1) The Optical Effect of the Side Dopant Window Position: In Section V-D-2), the spacing parameter "A" between the side dopant window and the rib edge was shown to have a tremendous effect on the modulator operating bandwidth. When "A" has a value of 50 nm (RM), the optical modulator has superior switching characteristics when compared with devices having a larger value of "A". However, the device also suffers excessive optical absorption of the propagating optical mode. Fig. 15 shows the relationship between the optical power and the side dopant spacing for the optical modulator in Fig. 1. As can be seen from Fig. 15, the RM introduces a high attenuation to the optical signal because the contact spacing is small.

From Fig. 15, the optical attenuation introduced to the modulator reaches a plateau when "A" is approximately 1.5 μm. This implies that at values of "A"$\geq$ 1.5 μm, the modulator experiences minimal optical attenuation due to the n^+ contacts. Hence, by choosing "A" to be 1.5 μm and performing a similar study for the p^+ dopant depth at the top of the rib, an optical modulator that has minimal optical loss can be selected. Fig. 16 shows the relationship between the optical output power and the top-rib doping depth.

An alternative device with side-doping contacts 1.5 μm from the rib edge (i.e., "A"$=$ 1.5 μm) and a rib doping depth of 0.1 μm introduces approximately 0.43 dB of passive loss for

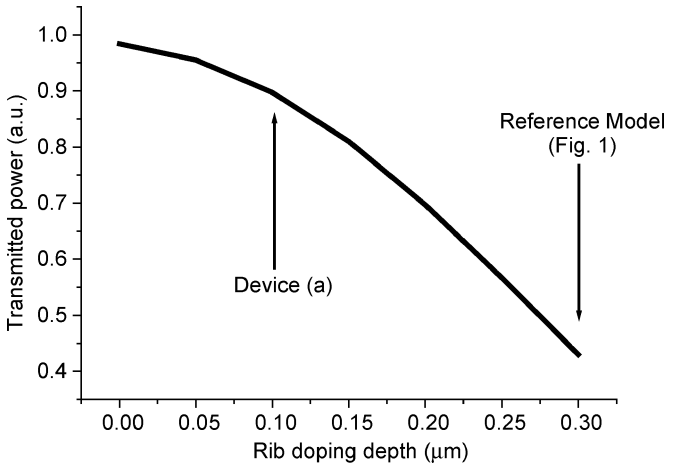

Fig. 16. Optical output power with varying values of rib doping depth. The value of the parameter "A" (Fig. 1) is taken to be 1.5 μm.

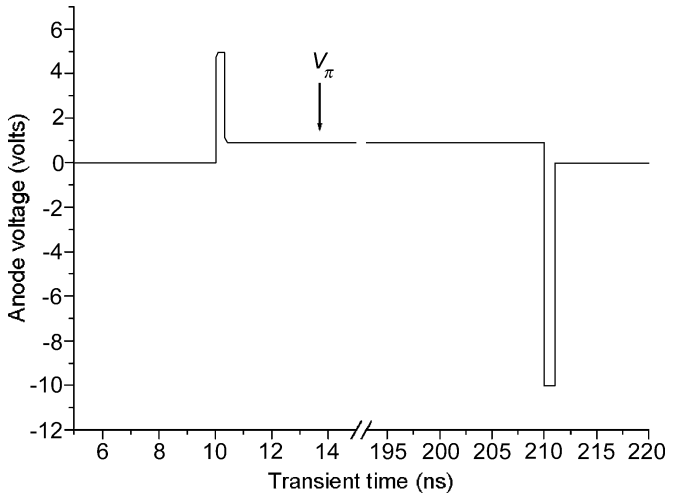

Fig. 17. Alternative switching waveform applied to Device (a). The magnitude of the waveform at the rise and fall times was derived after determining the optimum voltage necessary for the lowest switching times.

a 500-μm-long device. This "new" device is expected to operate in the region of approximately 95 MHz with a drive current requirement of the order of approximately 15 mA. This is a clear demonstration of a tradeoff between the power consumption and the device operating speed with respect to the spacing between the side dopant window and the rib edge. An alternative electrical injection method is introduced in the next section to significantly improve the electrical operating characteristics of such a device. This "new" device is termed *Device (a)*.

VI. Alternative Electrical Switching

Device (a) is predicted to operate in the range of approximately 95 MHz ($t_r = 5.25$ ns), and although this speed is more than seven-fold faster than current silicon-based optical phase modulators reported as typically 13 MHz (e.g., [7]), it is still low compared to the operating speed of compound materials which operate in multi-gigahertz regime (e.g., [19]). Consequently, further work has been carried out to try to improve this situation. This section discusses an alternative electronic drive waveform to enhance device speed.

A. Determination of Switching Waveform

In all the previous transient analysis, a rectangular pulse is applied to the device, and the limiting switching parameter is the rise time t_r. We can improve the response time of the modulator using an alternative driving waveform.

Determination of this waveform was made as follows: in order to decrease t_r, an extremely short pulse (of the order of picoseconds) was applied to the anode to switch from 0 V to a voltage approximately five times V_π. Doing so results in a faster injection of the electrons and holes into the intrinsic region via the larger applied field, thus reducing the rise time. Similarly, to improve the fall time, the same principle was applied to the falling edge of the waveform, and it is concluded that the optimum fall time would result when a negative voltage of approximately ten times the π-phase shift voltage V_π is applied. Fig. 17 depicts this waveform. Using this switching waveform allows us to obtain a switching speed of more than 5.8 GHz ($t_r = 85$ ps) compared with the typical switching frequency of Device (a), which is of the order of 95 MHz. Clearly, there are some difficulties in generating the waveform of Fig. 17, but the increased device speed is very significant.

B. Ramifications of the Fast Switching Waveform

The switching result generated by the waveform is extremely promising as it offers the possibility of active silicon optical phase modulators starting to compete with costly compound materials used traditionally in high-speed modulation devices. However, there are a number of points that must be noted in connection with this proposed switching.

The first is the amount of charge switched within the device during the rise and fall sections of the waveform. The peak current corresponding to the rise time for a conventional square wave drive is approximately 24 mA/μm compared with approximately 500 mA/μm for the fast switching waveform. Such high levels of current are clearly problematic.

The second point concerns the drive circuitry. In order to achieve rise times of the order of tens of picoseconds and at such high voltage levels, the design of the drive circuitry is complex and must be capable of switching such high currents in very short times.

VII. Conclusion

The plasma dispersion effect offers a means for electrically controlled optical modulation in a silicon waveguide. It has been shown that efficient phase modulation can be achieved in silicon by use of a p-i-n diode structure to inject charge carriers into an SOI waveguide. We have predicted that by using small geometry optical modulators, gigahertz modulation bandwidth could be achieved for a driving current of $\sim$1.5 mA.

This paper analyzed the device characteristics using a 2-D semiconductor simulation package SILVACO to investigate the dc and transient behavior of the active region of the modulator.

The paper also studied the effects of rounded rib edges, doping profiles and concentrations, diffusion depths, and alignment of the doped regions, on both the static and dynamic behavior of the phase modulator. The results indicate that

the dc modulator performance depends mostly on the doping profile, concentration, and dopant depth of the n^+ and p^+ doped regions, whereas the dynamic behavior is influenced by both the lateral displacement of the n^+ regions and the depth of the p^+ region.

These predicted results are very promising and indicate scope for further optimization of experimental devices. While this paper discusses the results of a specific phase modulator design, the results suggest that deep contacts and close lateral separation of the contacts would also enhance the performance of other p-i-n phase modulator geometries, although there would clearly need to be a specific evaluation of any given design.

The optical characteristics of the phase modulator was also analyzed with specific attention to its side dopant placement from the rib base, and it was concluded that the position of the side contact is a compromise between device speed and loss. We have proposed a switching waveform that is predicted to increase the device speed of one specific design from 95 MHz to more than 5 GHz.

ACKNOWLEDGMENT

C. E. Png would like to thank the Overseas Research Student (ORS) Award Scheme, Bookham Technology, Inc., and the Institution of Electrical Engineers (IEE) for funding his Ph.D. studies. S. P. Chan and S. T. Lim would like to thank Agilent Technologies (Singapore) and the University of Surrey, Surrey, U.K., for funding in part their Ph.D. studies.

REFERENCES

[1] SILVACO International, , Santa Clara, CA.
[2] A. G. Rickman, G. T. Reed, and F. Namavar, "Silicon-on-insulator optical rib waveguide loss and mode characteristics," *J. Lightwave Technol.*, vol. 12, pp. 1771–1776, Oct. 1994.
[3] A. G. Rickman and G. T. Reed, "Silicon-on-insulator optical rib waveguides: Low mode characteristics, bends and y-junctions," *Inst. Elect. Eng. Proc. Optoelectronics*, vol. 141, pp. 391–393, 1994.
[4] J. Schmidtchen, A. Splett, B. Schuppert, and K. Petermann, "Low-loss single-mode optical waveguides with large cross section in silicon-on-insulator," *Electron. Lett.*, vol. 27, pp. 1486–1487, 1991.
[5] T. W. Ang, P. D. Hewitt, A. Vonsovici, G. T. Reed, A. G. R. Evans, P. R. Routley, T. Blackburn, and M. R. Josey, "Integrated optics in unibond for greater flexibility," in *Proc. Electrochemical Soc.*, vol. 99, 1999, pp. 353–360.
[6] R. A. Soref and J. P. Lorenzo, "All-silicon active and passive guided-wave components for $\lambda = 1.3$ μm and 1.6 μm," *IEEE J. Quantum Electron.*, vol. QE-22, pp. 873–879, June 1986.
[7] P. D. Hewitt and G. T. Reed, "Improving the response of optical phase modulators in SOI by computer simulation," *J. Lightwave Technol.*, vol. 18, pp. 443–450, Mar. 2000.
[8] C. K. Tang and G. T. Reed, "Highly efficient optical phase modulator in SOI waveguides," *Electron. Lett.*, vol. 31, pp. 451–452, Mar. 1995.
[9] A. Vonsovici and A. Koster, "Numerical simulation of a silicon-on-insulator waveguide structure for phase modulation at 1.3 μ m," *J. Lightwave Technol.*, vol. 17, pp. 1–7, Jan. 1999.
[10] R. A. Soref and B. R. Bennett, "Kramers-Kronig analysis of E-O switching in silicon," *SPIE Integrated Opt. Circuit Eng.*, vol. 704, pp. 32–37, 1986.
[11] ——, "Electrooptical effects in silicon," *IEEE J. Quantum Electron.*, vol. QE-23, pp. 123–129, Jan. 1987.
[12] R. A. Soref, J. Schmidtchen, and K. Petermann, "Large single-mode rib waveguides in GeSi-Si and Si-on-SiO_2," *IEEE J. Quantum Electron.*, vol. 27, pp. 1971–1974, Aug. 1991.
[13] C. K. Tang, G. T. Reed, A. J. Walton, and A. G. Rickman, "Low-loss, single-mode, optical phase modulator in SIMOX material," *J. Lightwave Technol.*, vol. 12, pp. 1394–1400, Aug. 1994.
[14] C. E. Png, G. Masanovic, and G. T. Reed, "Coupling to 1 μm silicon modulators," *Proc. SPIE Photonics West*, vol. 4654, pp. 62–69, 2002.
[15] A. Cutolo, M. Iodice, P. Spirito, and L. Zeni, "Silicon electro-optic modulator based on a three terminal device integrated in a low-loss single-mode SOI waveguide," *J. Lightwave Technol.*, vol. 15, pp. 505–518, Mar. 1997.
[16] BeamPROP, Rsoft, Inc., Research Software, Ossining, NY.
[17] A. Sakai, T. Fukazawa, and T. Baba, "Low loss ultra-small branches in a silicon photonic wire waveguide," *IEICE Trans. Electron.*, vol. E85-C, pp. 1033–1038, 2002.
[18] K. K. Lee, D. R. Lim, H. Luan, A. Agarwal, J. Foresi, and L. C. Kimerling, "Effect of size and roughness on light transmission in aSi/SiO_2 waveguide: Experiments and model," *Appl. Phy. Lett.*, vol. 77, pp. 1617–1619, 2000.
[19] R. Spickermann, N. Dagli, and M. G. Peters, "GaAs/AlGaAs electro-optic modulator with bandwidth $>$40 GHz," *Electron. Lett.*, vol. 31, pp. 915–916, 1995.

Ching Eng Png was born in Singapore in 1974. He received the B.Eng. degree in electronic and electrical engineering (First-Class Hons.) from the University of Surrey, Surrey, U.K., in 1999. He is currently working toward the Ph.D. degree in the area of silicon-based integrated optics under the supervision of Prof. G. T. Reed at the same university.

He worked in Agilent Technologies (Singapore) from November 1999 to September 2000 as a New Product Introduction Engineer (NPI) in Gigabit Optical Transceivers. His current research interests include silicon-on-insulator (SOI) waveguides and silicon-based photonics.

Mr. Png was awarded an industrial sponsorship by Bookham Technology, Inc., and the Overseas Research Scholarship (ORS) Award Scheme in October 2000 to pursue the Ph.D. degree. He was recently awarded the Royal Academy of Engineering Prize at the House of Commons, Palace of Westminster, London, U.K., and named an Institution of Electrical Engineers (IEE) Hudswell International Research Scholar for his work on silicon optical modulators.

Seong Phun Chan was born in Malaysia in 1976. He received the B.Eng. degree (Hons.) from the School of Electronics and Physical Sciences, University of Surrey, Surrey, U.K., in 2000. He is currently working toward the Ph.D. degree under the supervision of Prof. G. T. Reed at the same university.

His research interests include integrated optics in silicon-on-insulator (SOI), waveguide-based Bragg grating devices, and thermooptic phenomena in SOI waveguides.

Mr. Chan was awarded a scholarship from Agilent Technologies (Singapore) in October 2000 to pursue the Ph.D. degree.

Soon Thor Lim was born in Singapore in 1975. He received the B.Eng. degree in electrical and electronic engineering (First-Class Hons.) from the University of Surrey, Surrey, U.K., in 2000. He is currently working toward the Ph.D. degree in silicon photonics with particular emphasis on design and modeling arrayed waveguide grating (AWG) under the supervision of Prof. G. T. Reed at the same university.

He was awarded a scholarship from Agilent Technologies (Singapore) in 2001 to pursue the Ph.D. degree.

Graham T. Reed received the B.Sc. degree in electronic and electrical engineering (First-Class Hons.) and the Ph.D. degree in integrated optics from the University of Surrey, Surrey, U.K., in 1983 and 1987, respectively.

He joined the University of Surrey in 1989 with the aim of establishing a research activity in guided-wave optoelectronics and now leads an internationally recognized group. He is responsible for initiating a new research field in the United Kingdom on silicon integrated optical circuits. His group has produced a series of leading technical advances in the field worldwide, notably in optical modulators, grating couplers, and optical sensing applications, which has been adopted by Bookham Technology, Inc., as its core business during the early 1990s and has been associated with companies and universities in the United Kingdom, the United States, France, Italy, Germany, Japan, and Singapore. He continues to publish his work and has contributed to more than 80 publications in the field of guided-wave optoelectronics.